View metadata, citation and similar papers at core.ac.uk
brought to you by CORE
provided by Ghent University Academic Bibliography

Thin film solid-state reactions forming carbides as contact materials for carbon-containing semiconductors

W. P. Leroy,[a] C. Detavernier,[b] and R. L. Van Meirhaeghe
Vakgroep Vaste-Stofwetenschappen, Ghent University, Krijgslaan 281/S1, B-9000 Gent, Belgium

C. Lavoie[c]
IBM T. J. Watson Research Center, Yorktown Heights, New York 10598
and Engineering Physics Department, Ecole Polytechnique de Montréal, Montréal, Quebec, Canada

(Received 12 September 2006; accepted 30 December 2006)

Metal carbides are good candidates to contact carbon-based semiconductors (SiC, diamond, and carbon nanotubes). Here, we report on an *in situ* study of carbide formation during the solid-state reaction between thin films. The solid-state reaction was examined between 11 transition metals (W, Mo, Fe, Cr, V, Nb, Mn, Ti, Ta, Zr, and Hf) and an amorphous carbon layer. Capping layers (C or TiN) of different thicknesses were applied to prevent oxidation. Carbide formation is evidenced for nine metals and the phases formed have been identified (for a temperature ranging from 100 to 1100 °C). W first forms W_2C and then WC; Mo forms Mo_2C; Fe forms Fe_3C; Cr first forms metastable phases Cr_2C and Cr_3C_{2-x}, and finally forms Cr_3C_2; V forms VC_x; Nb transforms into Nb_2C followed by NbC; Ti forms TiC; Ta first forms Ta_2C and then TaC; and Hf transforms into HfC. The activation energy for the formation of the various carbide phases has been obtained by *in situ* x-ray diffraction. © *2007 American Institute of Physics*. [DOI: 10.1063/1.2561173]

I. INTRODUCTION

Several carbon-based semiconductors are promising materials for electronic applications. SiC and doped diamond are superior wide-band-gap semiconductors, offering a high breakdown voltage, high thermal conductivity, small dielectric constant, and excellent radiation hardness.[1,2] Carbon nanotubes (CNTs) are quasi-one-dimensional molecular structures with semiconducting or metallic properties, which are widely investigated for application in the field of nanoelectronics.[3] To take advantage of these promising properties, there is a need for reliable contacts to these carbon-containing semiconductors.

In silicon-based technology, metal-silicon compounds (silicides) are now widely used as contact materials, since they offer several advantages as compared to metal contacts. Firstly, unlike pure metals several silicide phases are thermodynamically stable in contact with silicon. Secondly, when silicides are formed by a solid-state reaction between metal and Si, contact formation can be achieved by means of a self-aligned process (SALICIDE).[4] The solid-state reaction between the thin metal film and Si only occurs in those regions of a patterned substrate, where the metal is in direct contact with the Si (or C for the present case of carbides). Therefore, there is no need for alignment and lithographic patterning of the metal film, since the formation of the silicide will be automatically restricted to the contact region. One can expect the same advantages when using carbides to contact carbon-based semiconductors.

Carbides (i.e., metal-carbon compounds) are well known due to some of their unusual physical and chemical properties. The extreme hardness[5] and high melting point make carbides attractive materials for cutting and grinding tools, but they are also researched as potential catalysts.[6,7] Table I gives some basic properties of the carbide phases relevant to this work. The first column gives the resulting thickness for the carbide phase obtained when starting from 1 nm of metal to form the phase (i.e., a measure for the carbon consumption). The thicknesses were calculated[8] using the x-ray diffraction (XRD) densities,[9] crystal structure, and number of atoms. Other properties given are the crystal structure, the melting point, the formation enthalpy, the resistivity, the thermal expansion coefficient, and the Young's modulus.

The fact that these hard materials are also electronic conductors has more recently led to a research interest on microelectronic applications for carbides.[10] For instance, Schaper *et al.*[11] have reported on the role of iron carbide in the growth of multiwalled CNTs. Examples of carbides used as contact materials are already available in the literature: WC was examined as a schottky contact to 6H–SiC (Ref. 12) and to diamond;[13] TiC was used as an Ohmic contact to 6H–SiC,[14] but also as an Ohmic contact to diamond[15] and CNTs.[16]

Contact materials are usually evaluated on (a) their thermodynamic stability in contact with the semiconductor, (b) their electric conductivity (as high as possible), (c) their formation temperature (as low as possible), and (d) their contact resistance (as low as possible). Adhesion and mechanical properties of the contact material and thermal expansion mismatch between contact and substrate, should also be considered in the evaluation of contact materials. Therefore, the thermal expansion coefficient and Young's modulus of the different carbide phases are listed in Table I.

[a]Electronic mail: Wouter.Leroy@UGent.be
[b]Electronic mail: Christophe.Detavernier@UGent.be
[c]Electronic mail: CLavoie@us.ibm.com

 © 2007 American Institute of Physics

PROOF COPY 100704JAP

AQ: #7

TABLE I. Literature overview of the basic properties of the different carbide phases. The carbide thickness was calculated from crystallographic data, using the method described by Chen (Ref. 8). The melting points (MP), the formation enthalpies, the resistivities, thermal expansion coefficients, and the Young's modulus were obtained from different sources.

Carbide phase	Thickness (nm/nm metal)	Structure	MP[a] (°C)	Formation enthalpy (kJ/mole)	Resistivity ($\mu\Omega$ cm)	Thermal expansion[a,b] (10^{-6}/°C)	Young's modulus[a] (GPa)
W_2C	1.16	hcp	2800	−52.7[a,b]	80[a]		
WC	1.31	Simple hexagonal	2750	−40.5,[b] −35.1[a,c]	22,[b] 25[a]	5.0∥∣,[b] 4.2∥[c]	670
Mo_2C	1.19	hcp	2410	−46.0,[b] −92.0,[a] −49.0[c]	71[a]	4.9∥,[b] 8.2∥[c]	228
Fe_3C	1.10	Orthorombic	1650	31.4,[a] 24.9[c]			
Cr_2C	1.24						
Cr_3C_2	1.23	Orthorombic	1895	−69.0,[b] −131.8,[b] −103.0[c]	75[a]	10.3	386
VC	1.43	fcc	2830	−102.5[a,c]	60,[a,b] 65[b]		434
Nb_2C	1.17	hcp	3100	−194.5,[b] −376.6,[a] −145.6[c]			
NbC	1.18	fcc	3480	−140.5,[b] −138.1[a]	35,[a,b] 51.1[b]	6.6	510
$Mn_{23}C_6$	1.05	Complex cubic	1010				
Mn_3C		Orthorombic	1520	−288.7,[a] −15.6[c]			
TiC	1.14	fcc	3140	−184.5,[b] −238.5,[a] −186.2[c]	68[a]	7.6	448
Ta_2C	1.14	hcp	3400	−208.4,[b] −384.9,[a] −197.5[c]			
TaC	1.21	fcc	3880	−142.7,[b] −159.0,[a] −150.6,[c]	25,[a,b] 42.1[b]	6.3	365
ZrC	1.16	fcc	3550	−196.6,[b,c] −200.8[a]	42,[b] 63[a]	6.7	386
HfC	1.11	fcc	3890	−209.5,[b] −338.9,[a] −226.8[c]	37[a,b]	6.6	462

[a]Reference 48.
[b]Reference 47.
[c]Reference 49.

PROOF COPY 100704JAP

84 In this work, 11 carbide forming metals (Ti, V, Cr, Mn, 85 Fe, Zr, Nb, Mo, Hf, Ta, and W) are examined in a solid-state 86 thin film reaction with amorphous carbon. Not all metals 87 form a carbide, when reacted with carbon. From the binary 88 phase diagrams[17] we have selected the 11 transition metals 89 listed above, as carbide-forming metals. Existing literature 90 on the formation of carbides using solid-state reactions is 91 limited to annealing times of one hour and more, followed by 92 *ex situ* measurements.[18,19] Although this gives evidence that 93 a certain phase has formed, there is little information on the 94 kinetics of the process. In this work, a technique was used to 95 observe the solid-state reaction *in situ*, i.e., during annealing.

96 II. EXPERIMENT

97 The 11 transition metal candidates (Ti, V, Cr, Mn, Fe, Zr, 98 Nb, Mo, Hf, Ta, and W) were deposited on a sputter depos- 99 ited amorphous carbon layer of 200 nm on SiO_2 wafers. The 100 30 nm metal layers were sputter deposited at a base pressure 101 of 10^{-6} mbar. Cr, Mn, and V were also deposited using *e*-gun 102 evaporation at a pressure of 10^{-5} mbar. The samples were 103 first made without a top layer, but in attempts to prevent 104 oxidation, different capping layers were applied: first, a 5 nm 105 C capping layer, and later, 30 nm C or TiN was used.

106 The reaction between a thin metal film and a carbon 107 substrate was investigated using *in situ* XRD for phase iden- 108 tification and for determining the activation energy E_a, four- 109 points probe for resistance measurements, x-ray photoelec- 110 tron spectroscopy (XPS) for phase composition information, and Rutherford backscattering spectroscopy (RBS) for con- 111 tamination and thickness measurements. 112

The *in situ* XRD experiments were performed at the 113 X20C beamline of the National Synchrotron Light Source 114 (NSLS) at Brookhaven National Laboratory. During anneal- 115 ing, the sample is continuously illuminated by an intense 116 beam of monochromatic x rays ($\lambda = 0.177 - 0.180$ nm). Dur- 117 ing the measurement, the samples were heated from 118 100 to 1100 °C in a purified He atmosphere, at different 119 ramp rates (from 0.3 to 35 °C/s). Diffracted photons from 120 the sample are continuously detected by an array of photo- 121 diodes covering 14° in 2θ. Acquisition times can vary from 122 100 ms to several seconds depending on the annealing con- 123 ditions. For the standard heating rate of 3 °C/s presented 124 here, a spectrum is taken every 0.5 s. 125

III. RESULTS 126

A. W–C 127

Figure 1 shows a part of the 2θ spectrum when anneal- 128 ing at 3 °C/s to 1150 °C. Around 200 °C, there is a phase 129 change from β-W to α-W. This does not affect the carbide 130 formation, as was confirmed by *in situ* measurements of 131 solid-state reactions, starting from α-W. One observes a 132 clear phase transition from W [observe the W(110) peak in 133 Fig. 1] to W_2C in the temperature range of 920–970 °C. 134 One cannot tell whether this metal-rich carbide phase is the 135 hexagonal phase or the orthorhombic phase, as, respectively, 136 the (110), (002), $(\bar{1}\bar{1}1)$ and the (002), (200), (102) peaks of 137

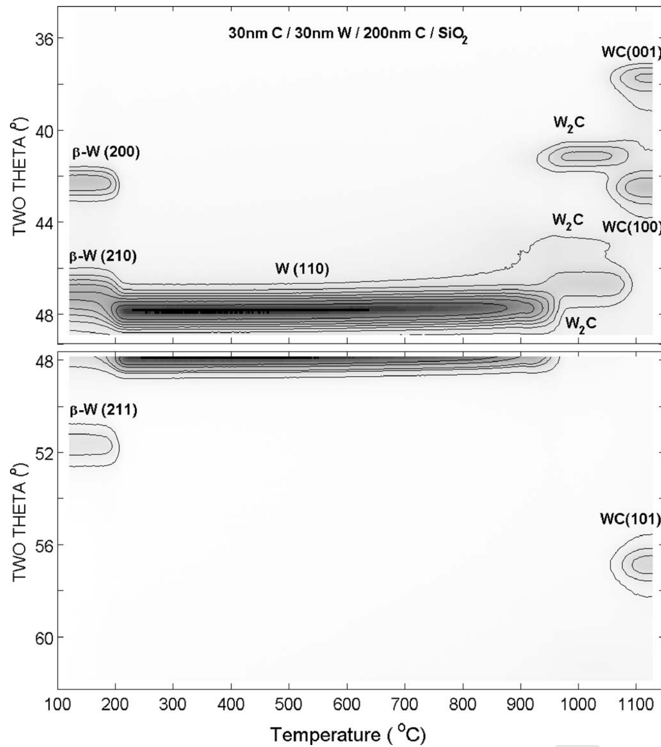

FIG. 1. *In situ* XRD pattern of 30 nm W on 200 nm C on SiO_2 with 30 nm C capping layer; $2\theta \approx 35°$ to $\approx 61°$, annealed in He atmosphere from 100 to 1150 °C at 3 °C/s.

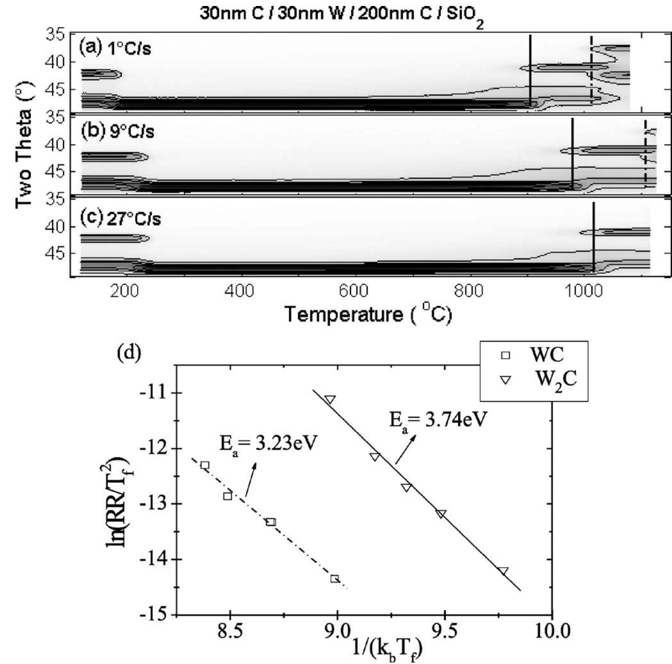

FIG. 2. *In situ* XRD measurements on a W–C system with 30 nm C capping layer at heating rates of 1 °C/s (a), 9 °C/s (b), and 27 °C/s (c). The lines on the XRD measurements show the shift towards higher temperatures, when the heating rate is increased (full lines for W_2C, dash-dot lines for WC). The bottom figure (d) shows a linear fit to obtain the activation energy, following Eq. (1). From the fit follows $E_a^{W_2C} = 3.74 \pm 0.33$ eV ($R = 0.9952$) for W_2C formation and $E_a^{WC} = 3.23 \pm 0.41$ eV ($R = 0.9932$) for WC formation.

the different crystal types coincide. From 1050 to 1100 °C the metal-rich carbide phase transforms into the hexagonal monocarbide WC. In Fig. 1 the (001), (100), and (101) peaks are identified. Figure 1 shows data for samples with a 30 nm C capping layer. The same experiments were done for samples without a capping layer. The same two carbide phases were found, although the temperature of the phase transitions were slightly higher.[20] Both carbide phases have been confirmed with RBS. Bachli *et al.*[19] reported on tungsten carbide formation on polycrystalline diamond, and found the same phase sequence (first W_2C, then WC).

As explained by Colgan and d'Heurle,[21] the activation energy E_a can be determined from ramped *in situ* measurements, using a Kissinger-like method. To obtain the activation energy, *in situ* XRD measurements are done at different heating rates (1, 3, 5, 9, and 27 °C/s), and for each heating rate, the transition temperature is determined. In our calculations, the maximum of the first derivative of the intensity of the XRD peak was used as the transition temperature. As shown in Fig. 2 for the W–C system, the transition temperature shifts towards higher values, when the ramp rate is increased. This is clearly demonstrated in Fig. 2(c), where the transition from W_2C to WC does not take place in the measured temperature range (100–1150 °C), at a heating rate of 27 °C/s. Using the equation[21]

$$ln\left[\frac{dT/dt}{T_f^2}\right] = -\frac{E_a}{k_b T_f} + C, \quad (1)$$

AQ: #2

with dT/dt the ramp rate, T_f the formation temperature, and k_b the Boltzmann constant, the activation energy can be determined from the slope of the straight line obtained by plotting $\ln[(dT/dt)/T_f^2]$ vs $1/k_b T_f$ for the different ramp rates and the respective transition temperatures. This is shown in Fig. 2(d). In the remainder of this paper, the correlation coefficient (R) will be supplied with the values for the activation energy as an indication for the scatter of the data points from the fitted line, instead of showing every single Kissinger plot. Apart from this statistical error related to the curve fitting, a more important error originates from the temperature registration in each measurement. Because of this, each transition temperature has an error of ±3 °C, which will give a variation (an error) on the calculated activation energy.

For the W–C system we obtained an activation energy $E_a^{W_2C} = 3.74 \pm 0.29$ eV ($R = 0.9952$) for W_2C formation, and $E_a^{WC} = 3.23 \pm 0.29$ eV ($R = 0.9932$) for WC formation. Bushmer and Crayton[22] studied the self-diffusion of ^{14}C into WC, and obtained an activation energy $E_a^{b.d.} = 3.82$ eV for bulk diffusion, and $E_a^{g.b.d.} = 3.08$ eV for grain-boundary diffusion. The sheet resistance was measured with a four-point probe, and the resistivities $\rho^{W_2C} \approx 114$ $\mu\Omega$ cm and $\rho^{WC} \approx 300$ $\mu\Omega$ cm were obtained, using the calculated thicknesses of 34.8 and 39.4 nm for the metal-rich carbide and the monocarbide, respectively. Romanus *et al.*[23] found values for the resistivity ranging between 100 and 340 $\mu\Omega$ cm for different WC–W_2C mixtures.

B. Fe–C

For the Fe–C system, Fig. 3 shows the formation of the Fe_3C carbide in a temperature range of 550–590 °C. The same experiments were performed on samples with a capping layer. As remarked above, the transition temperature

COPY 100704JAP

PROOF COPY 100704JAP

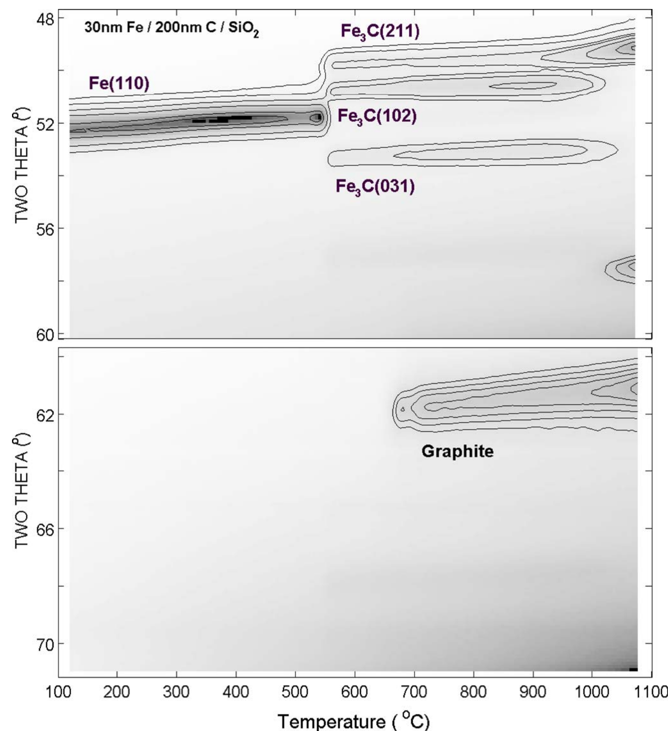

FIG. 3. *In situ* XRD pattern of 30 nm Fe on 200 nm C on SiO_2, $2\theta \approx 47°$ to $\approx 71°$, annealed in He atmosphere from 100 to 1100 °C at 3 °C/s.

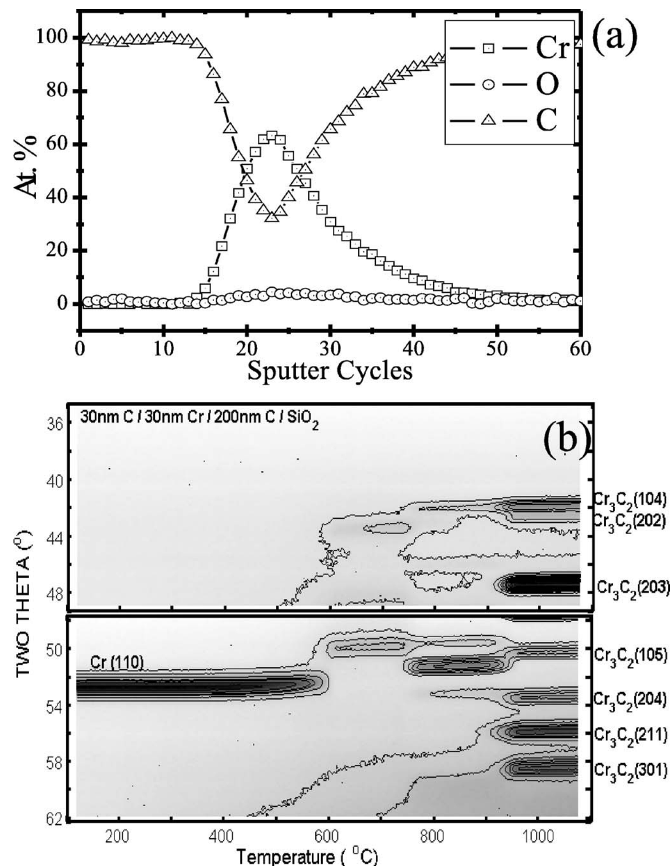

FIG. 4. (a) An XPS depth profile of an as-deposited sample. (b) *In situ* XRD pattern of 30 nm Cr on 200 nm C on SiO_2 with a 30 nm C capping layer, $2\theta \approx 35°$ to $\approx 62°$, annealed in He atmosphere from 100 to 1100 °C at 3 °C/s.

196 shifts to slightly lower temperatures for samples with a cap-
197 ping layer (510–550 °C). Santaniello *et al.*[24] irradiated Fe
198 layers on high-purity pyrolitic graphite with D^+ beams at
199 temperatures ranging from room temperature to 1100 K
200 (827 °C), and their results suggest a carbide formation
201 around 800 K (527 °C).

202 We used *in situ* XRD to determine the activation energy
203 for the formation of Fe_3C and found $E_a^{\mathrm{C\ cap}} = 4.05 \pm 0.83$ eV
204 ($R = 0.9941$) for samples with a 30 nm C capping layer, and
205 $E_a^{\mathrm{no\ cap}} = 2.9 \pm 0.27$ eV ($R = 0.9898$) for samples without cap-
206 ping layer.

207 In Fig. 3, a special feature can be observed around
208 630 °C at $2\theta \approx 61°$. RBS measurements confirmed that a
209 carbon layer on top of the carbide has formed, and it should
210 be stressed that this segregation occurs, even for samples
211 without an as-deposited C capping layer. Santaniello *et al.*
212 report[24,25] the segregation of a carbon layer on top of Fe
213 films. Sinclair *et al.*[26] used trilayered samples, comparable to
214 the samples with a C capping layer used in this study. They
215 studied this graphite-forming behavior, and named it
216 "carbide-mediated graphitization." Jiang and Carter[27] predict
217 this segregation layer theoretically with density functional
218 theory (DFT) calculations. Therefore, we conclude that
219 around 630 °C; a graphite layer on top of the carbide layer
220 has formed with a diffraction peak at $2\theta \approx 61°$ [(004)] [there
221 is also a peak (002) at $2\theta \approx 29°$].

222 C. Cr–C

223 Cr–C is an interesting metallurgical system, as chro-
224 mium carbides act as strengthening precipitates in steels.
225 One of the differences compared to other systems is already
226 noticeable with the as-deposited sample. XPS depth profiling
227 (Fig. 4, inset) shows that C has already diffused into the Cr
228 metal layer. Sinclair *et al.*[26] showed the same effect using
229 cross-sectional transmission electron microscopy (TEM).
230 Upon annealing they found the formation of the metastable
231 hexagonal Cr_2C phase, followed by a second metastable
232 phase, orthorhombic Cr_3C_{2-x}, and finally the graphitization
233 of amorphous carbon. The orthorhombic metastable Cr_3C_{2-x}
234 phase was first identified by Bouzy *et al.*[28] Figure 4 shows
235 the *in situ* XRD patterns for the Cr–C system. The Cr(110)
236 peak disappears between 580 and 620 °C, and we see the
237 formation of a new phase. Additional *ex situ* XRD on a
238 sample quenched at 650 °C evidenced the coexistence of the
239 metastable carbide phase Cr_2C and the oxide CrO_2. At about
240 740–770 °C the next phase occurs, and can be identified as
241 Cr_3C_{2-x}. Between 900 and 950 °C the formation of the
242 stable Cr_3C_2 phase takes place. The phase sequence that was
243 observed with the *in situ* XRD is the same as reported by
244 Sinclair *et al.*,[26] although they did not observe the last phase,
245 the stable Cr_3C_2 carbide. Worth mentioning is the segrega-
246 tion of a graphite layer like in the Fe–C system. However,
247 the segregation here begins at quite a higher temperature:
248 around 930 °C (graphite peak not shown to save space). Sin-
249 clair *et al.* also observed the graphite formation for the Cr–C
250 system.

PROOF COPY 100704JAP

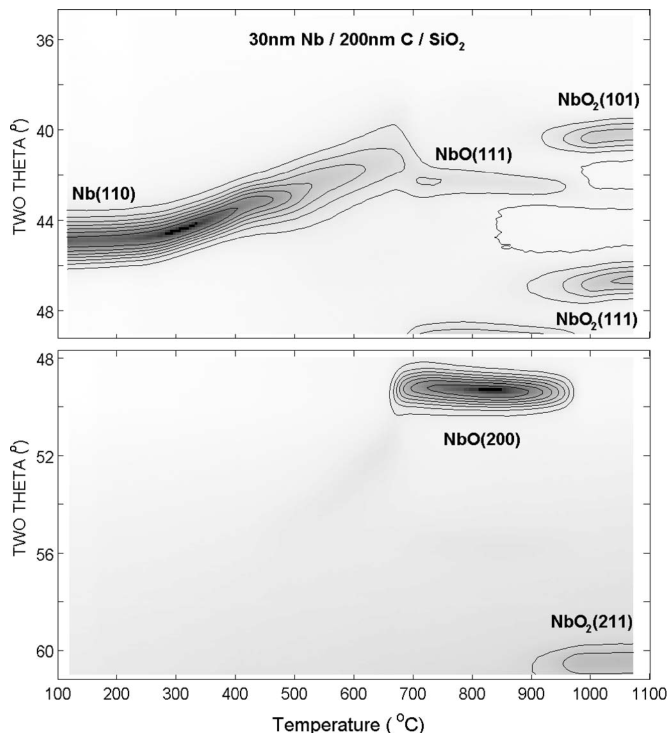

FIG. 5. *In situ* XRD pattern of 30 nm Nb on 200 nm C on SiO_2, for $2\theta \approx 35°$ to $\approx 61°$, annealed in He atmosphere from 100 to 1100 °C at 3 °C/s.

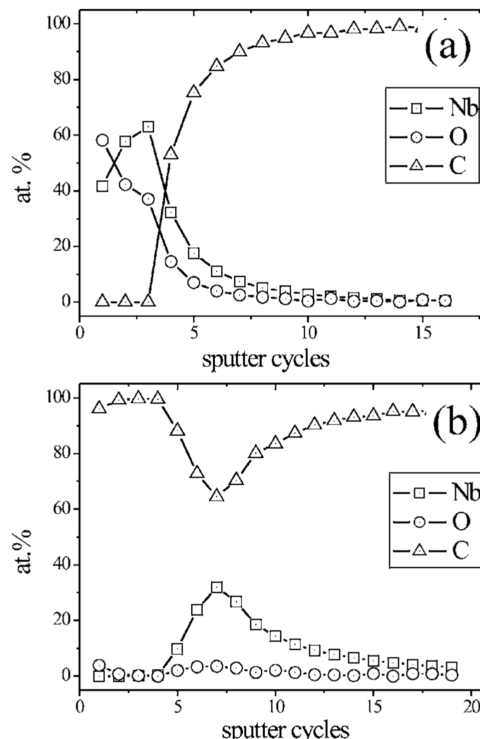

FIG. 7. XPS depth profiles of Nb–C system annealed to 850 °C, (a) without capping layer and (b) with 30 nm C capping layer.

D. Nb–C

When dealing with solid-state reactions to form carbides from thin films of metal and carbon, oxidation is an important factor to control. In Fig. 5, an *in situ* XRD pattern is shown for 30 nm Nb on 200 nm C, sputter deposited on a SiO_2 substrate. Around 700 °C the formation of NbO can be observed, followed by the formation of NbO_2 around 900 °C. The metal peak of Nb is clearly seen at the start of the experiment. However, upon annealing, the peak shifts towards lower 2θ values, which means that the d spacing of the lattice is increased. Because O atoms are diffusing interstitially into the metal lattice, the lattice (and therefore the d spacing) expands.

Figure 6 shows the solid-state reaction for the Nb–C system with a 30 nm C capping layer. From 690 °C, the hexagonal Nb_2C phase appears, with its (100), (002), and (101) peaks at $2\theta \approx 38.8°$, $\approx 42.4°$, and $\approx 44.4°$, respectively. This phase transition has not so definite boundaries as the next transition to the fcc monocarbide, NbC. From 880 to 940 °C, one observes the appearance of the (111) and (200) peaks of the NbC phase, at $2\theta \approx 40.7°$ and $\approx 47.4°$.

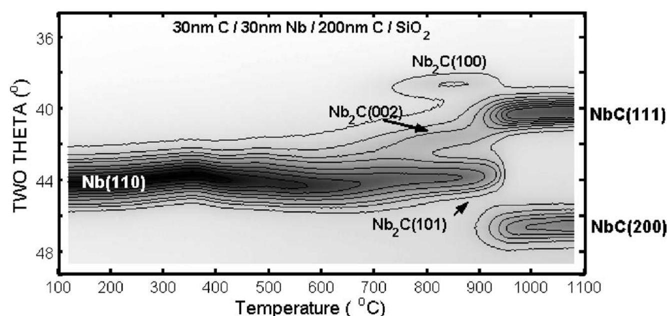

FIG. 6. *In situ* XRD pattern of 30 nm Nb on 200 nm C on SiO_2 with 30 nm of C as capping layer. $2\theta \approx 35°$ to $\approx 49°$, annealed in He atmosphere from 100 to 1100 °C at 3 °C/s.

The shift of the metal peak in the XRD plot for the uncapped sample is only an indication that oxidation might have occurred, but XPS (or RBS) gives more evidence. Figure 7 shows XPS depth profiles of samples that were quenched at 850 °C, (a) one without and (b) one with a capping layer. Looking at the oxygen concentration of both and combining these results with the XRD measurements, one can easily see that the Nb–C system has formed an oxide (NbO) when the system had no capping layer, and it formed a carbide (Nb_2C) when 30 nm C was applied as capping layer. Even more evidence for the carbide formation can be found in the single spectrum of the C 1s XPS peak. Ramqvist *et al.*[29] have shown that when a carbide is formed, the C 1s peak shows a *carbide* peak, shifted towards a lower binding energy, compared to the original C 1s position. They measured this shift for various carbides and concluded that this shift is a consequence of the transfer of electronic charge from the metal to the nonmetal constituent (here: carbon). For the case of Ti–C, they showed a shift of the metal Ti 2p peak towards a higher binding energy, when a carbide is formed. However, if an oxide is formed, the metal Ti 2p peak shifts in the same direction (to a higher binding energy) as when a carbide is formed, albeit over a different energy (depending on the oxide). Compared to that, if C–O bonds would be measured in the layer (C–O compounds are volatile, so difficult to observe), the C 1s peak would shift to a higher binding energy, thus in the opposite direction of when a carbide is formed. It is clear that one should pay close attention when examining solely the metal peak, and it is

COPY 100704JAP

PROOF COPY 100704JAP

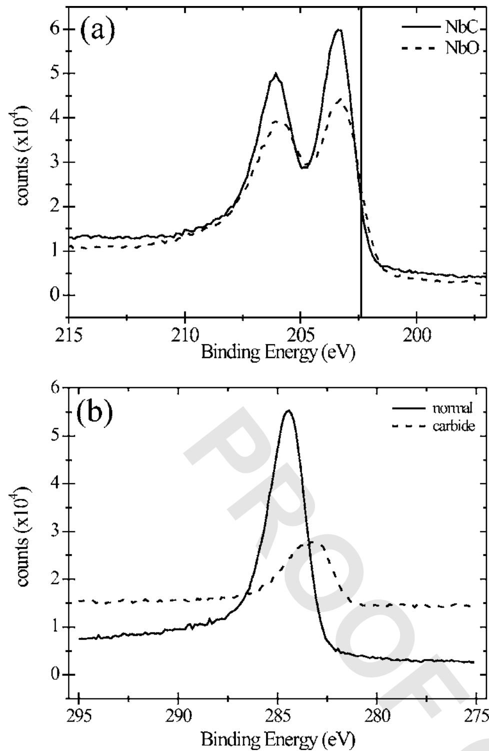

FIG. 8. (a) Nb 3d XPS spectra taken from a sample with a carbon capping layer and one from a sample without a capping layer, annealed to NbC and NbO, respectively. The full vertical line marks the position of the neutral Nb $3d_{5/2}$ peak. (b) C 1s XPS spectra selected out of an XPS depth profile of a Nb–C system with 30 nm C capping layer, annealed to 1050 °C. The full line shows the C 1s peak at its normal position, taken at a depth where no metal was present. The dashed line shows the C 1s peak at its "carbide" position, taken at a depth where C has reacted with Nb.

easier to examine the C 1s peak. As an example to this, Fig. 8(a) shows the Nb 3d peaks, one from an uncapped sample, the other from a capped sample, both annealed to 1050 °C, so the metal layers have reacted to NbO and NbC, respectively. There is almost no difference in peak position for both, and both have shifted to a higher binding energy, compared to the normal Nb binding energy. For this we have marked the normal position of the Nb $3d_{5/2}$ peak (the maximum of the right peak) with a full line on the graph. Figure 8(b) shows two single C 1s XPS spectra, one coming from a depth where no Nb was present, so where the carbon peak is at its normal position, and one from the reaction zone. It can be seen that the C 1s peak from the reaction zone has shifted towards a lower binding energy than the normal C 1s binding energy of 284.6 eV, so we conclude that a carbide has formed, not an oxide.

In our previous work,[20] we examined the influence of different capping layers to prevent oxidation. C capping layers of 5 and 30 nm thickness, and TiN layers of 30 nm thickness were used. Summarizing, the 30 nm C capping layer should give enough protection against oxygen in the annealing atmosphere. Also, these capping layers each influence the transition temperature to the carbide phase. This was observed, e.g., for the Mo–C system, which can also form its carbide phase without a capping layer. We stress that the capping layer should be made right after the metal deposition, without breaking the vacuum.

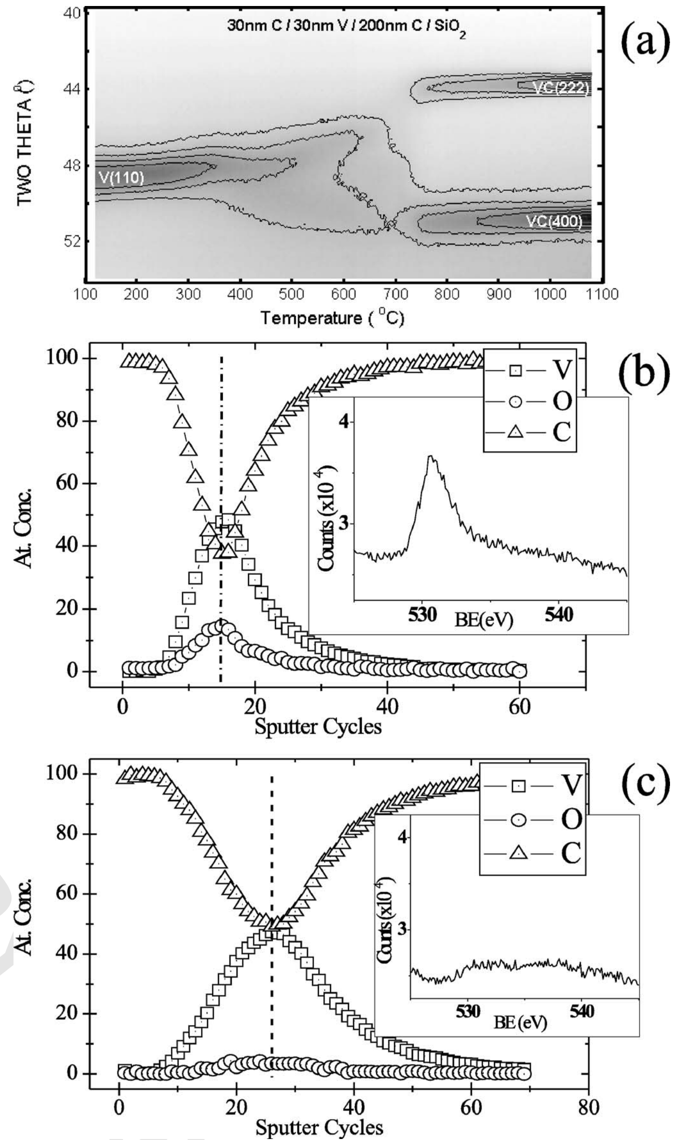

FIG. 9. *In situ* XRD pattern of 30 nm V on 200 nm C on SiO_2 with a 30 nm C capping layer, $2\theta \approx 40°$ to $\approx 54°$, annealed in He atmosphere from 100 to 1100 °C at 3 °C/s. (b) and (c) show XPS depth profiles of 30 nm V on 200 nm C with a 30 nm C capping layer, annealed to 600 °C (b) and to 1100 °C (c). The insets show the O 1s peak at the depth, marked with a line in the depth profile.

Activation energies for the two formed carbide phases are $E_a^{Nb_2C} = 3.01 \pm 0.36$ eV ($R = 0.9797$) and $E_a^{NbC} = 4.08 \pm 0.37$ eV ($R = 0.9879$), respectively. Guarnieri *et al.*[30] and Barzilai *et al.*[31] observed the same phase formation sequence for a 200 nm Nb layer on a diamond substrate and an 8 μm Nb layer on a graphite substrate, respectively. And although the latter researchers found lower activation energies for the Nb_2C and the NbC formations, namely, $E_a^{Nb_2C} = 1.97$ eV and $E_a^{NbC} = 1.70$ eV, our results are in the same range as many others.[30,32,33]

E. V–C

Figure 9(a) shows *in situ* XRD measurement for 30 nm V with a 30 nm C capping layer. The V (110) peak seems to split up around 400 °C and gradually moves towards $2\theta \approx 43.5°$ and $2\theta \approx 51°$. These have been identified as, respec-

PROOF COPY 100704JAP

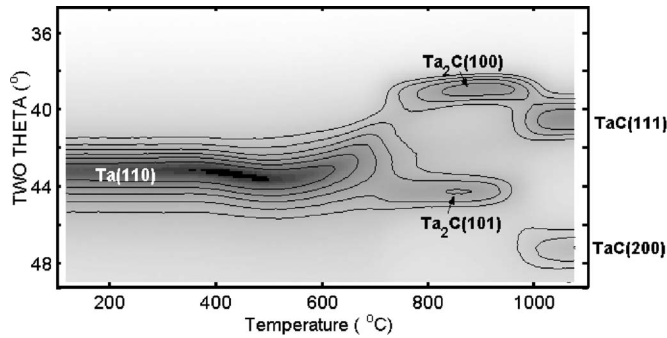

FIG. 10. *In situ* XRD measurements on Ta–C system with C capping layer. The peaks of the different phases are identified. The sample was annealed in He atmosphere from 100 to 1100 °C at 3 °C/s.

tively, the (222) and (400) peaks of a VC phase. From 680 to 730 °C this phase is formed and remains stable up to higher temperatures. *Ex situ* XRD identified the phase as $VC_{0.845}$. The activation energy for samples with a 30 nm C capping layer was determined as $E_a^{VC}=2.65\pm0.38$ eV ($R=0.9709$).

The shift of the metal peak towards lower 2θ values hints at the formation of an oxide, as explained above. However, an XPS measurement on a sample quenched at 1100 °C confirmed the formation of the monocarbide phase VC. For a sample quenched at 600 °C, a higher oxygen content was measured. Examination of the single spectra of the O 1*s* and C 1*s* peaks suggest that at this temperature, there already is some carbide formation, but it is mixed with an oxide. The O 1*s* peak was not present for the sample quenched at 1100 °C.

F. Ta–C

The Ta–C system exhibits similar oxidation problems as the Nb–C system, so a capping layer should be used to form a carbide phase. Figure 10 shows an *in situ* XRD measurement where the Ta(110) peak disappears, and the $Ta_2C(100)$ and $Ta_2C(110)$ peaks appear at $2\theta\approx39°$ and $\approx44.8°$, respectively. This transformation occurs between 690 and 750 °C. Between 950 and 1000 °C the metal-rich carbide phase forms the monocarbide TaC with (111) and (200) peaks at $2\theta\approx40.9°$ and $\approx47.6°$, respectively. XPS measurements confirm the formation of the monocarbide TaC. Although the phase sequence is correct, the formation temperatures given here are lower than they would be for a Ta–C system with 30 nm of metal. Measurements following the *in situ* experiment showed that the thickness calibration was off for this system, and a smaller layer of Ta was deposited (and examined). *Ex situ* measurements on samples with a corrected sample (30 nm Ta on 200 nm C, with 30 nm C capping layer) show the same phases forming, although the transition temperatures are higher. Unfortunately, *in situ* experiments were not available for this corrected sample. Because of this, the results for the thinner Ta–C sample are marked with a star in Table II.

Chen *et al.*[34] reported on the thermal reaction of Ta thin films (60–135 nm) with polycrystalline diamond. For the thinnest metal layer, they observed the phase formation of Ta_2C and TaC for 1 h annealing at 800 and 900 °C, respectively.

TABLE II. Experimental results for the carbide phases, formed through solid-state reaction of thin films. The formation temperature T_{form} was determined from *in situ* XRD measurements, at the standard heating rate of 3 °C/s. Only the formation temperature for samples with 30 nm C capping layer are given in the table. All carbide phases were formed, starting from samples with 30 nm of metal, except for the Ta–C system (marked with *), for which the thickness was less. the activation energy was calculated from *in situ* XRD measurements at different heating rates. The resistivity was measured *ex situ* using a four-point probe on quenched samples. The range of composition (*range of comp'n*) was estimated from the binary phase diagram.

Carbide phase	T_{form} (°C)	E_a (eV)	Resistivity ($\mu\Omega$ cm)	Range of comp'n MC_x ($0<x\leq1$)
W_2C	920–970	3.74±0.33	114	0.41–0.50
WC	1050–1100	3.23±0.41	300	=1
Mo_2C	700–770	3.15±0.27	59	0.47–0.50
Fe_3C	510–550	4.05±0.73	180	=0.25
Cr_2C	580–620			⋯
Cr_3C_{2-x}	740–770		72	⋯
Cr_3C_2	900–950		167	0.65–0.66
VC	680–730	2.65±0.24	214	0.74–0.92
Nb_2C	690	3.01±0.42	160	0.48–0.49
NbC	880–940	4.08±0.30	107	0.72–0.98
TiC	550–650	1.45±0.84	136	0.70–0.98
Ta_2C	690–750*		163	0.41–0.50
TaC	950–1000*		132	0.75–1
HfC	710–810	2.05±0.21	178	0.59–0.96

G. Zr–C

The *in situ* experiment for the Zr–C system with a capping layer is shown in Fig. 11(a) for $2\theta\approx35°$ to $\approx49°$. Around 300 °C a new peak arises at $2\theta\approx37.3°$, which could be the (100) peak of Zr. On the other hand, Zr_3O has peaks around the same positions of Zr. The formation of this oxide (Zr_2O, ZrO, and ZrO_2 do not have those XRD peaks) seems most plausible, as it is unlikely for a certain diffraction peak to appear and disappear again. Also, in the binary phase diagram of the Zr–O system Zr_3O is named α_3''Zr, indicating its close relationship to α-Zr. The Zr_3O seems to disappear again in favor of the metal, which in turn transforms to a next phase with peaks around $2\theta\approx38.5°$ and $\approx44.3°$. Around those 2θ values, both ZrO and ZrC have their (111) and (200) diffraction peaks. Therefore, XPS profiling should be used to determine whether an oxide or a carbide has formed. In Fig. 11(b) a depth profile on a sample annealed to 1100 °C is shown, and one can observe the high oxygen concentration in the layer, so the formation of ZrO is most probable. Inspecting the XPS C 1*s* spectra, a very small shift towards the "carbide" position was observed, as can be seen on the inset of Fig. 11(b), where the shoulder has been marked. We therefore conclude that a small amount of carbide has formed, but that oxidation of Zr was predominant, in spite of the presence of a capping layer.

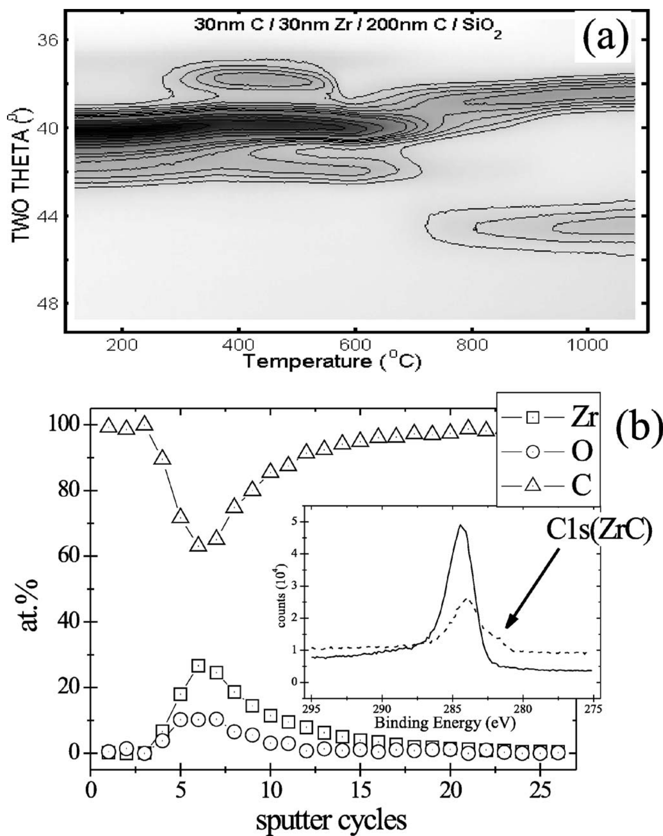

FIG. 11. (a) *In situ* XRD measurements on Zr–C system with C capping layer. The sample was annealed in He atmosphere from 100 to 1100 °C at 3 °C/s. (b) XPS depth profile on the same sample, after annealing. The inset shows XPS C 1*s* spectra, where a small peak at the "carbide" position hints some formation of ZrC.

H. Hf–C

The formation of the monocarbide HfC during the anneal of a 30 nm Hf layer with a 30 nm C capping layer, on an amorphous 200 nm C layer, can be seen in Fig. 12. Starting around 710 °C, the (111) and (200) peaks of HfC appear, and around 810 °C the transformation is complete. The capping layer is necessary to form the carbide. From *in situ* XRD measurements at different ramp rates, we have determined the activation energy for the HfC formation as $E_a^{\mathrm{HfC}} = 2.05 \pm 0.19$ eV ($R = 0.9749$).

I. Ti–C and Mo–C

The thin film solid-state formation of titanium carbide and molybdenum carbide is discussed in a previous paper.[20]

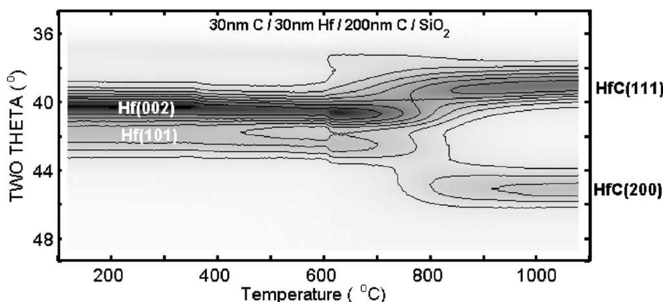

FIG. 12. *In situ* XRD pattern of 30 nm Hf on 200 nm C on SiO_2 with 30 nm of C as capping layer. $2\theta \approx 35°$ to $\approx 49°$, annealed in He atmosphere from 100 to 1100 °C at 3 °C/s.

In order to make the current report self-contained, we give an overview of the results, and include the activation energy for the TiC formation.

The Ti–C system is sensitive to oxidation (similar to Nb–C), and the formation of TiC occurred between 550 and 650 °C for samples with a 30 nm C capping layer. An activation energy $E_a = 1.45 \pm 0.81$ eV ($R = 0.7189$) was calculated.

The Mo–C system is less sensitive to oxidation. The transition to the Mo_2C phase was observed between 830 and 900 °C (no capping layer). Different capping layers were used, and the formation temperature varied significantly: $T_f^{5\ \mathrm{nm\ C}} = 730-800$ °C, $T_f^{30\ \mathrm{nm\ C}} = 700-770$ °C, and $T_f^{30\ \mathrm{nm\ TiN}} = 750-830$ °C. An activation energy was obtained for the Mo–C system with a 30 nm C capping layer, $E_a = 3.15 \pm 0.23$ eV ($R = 0.9968$).

IV. DISCUSSION

As mentioned before, the formation of carbides from thin films of metal and carbon is extremely sensitive to oxidation. We found that W, Mo, Fe, Cr, and V form a carbide, even when no capping layer is applied. The others (Nb, Ti, Ta, and Hf), however, need the C capping layer, or an oxide will form, instead of a carbide. As an example, this was discussed for the Nb–C system, and shown in Fig. 5. In Table III the elements are arranged with decreasing electronegativity. The metals last mentioned here (Nb to Hf) have a lower electronegativity compared to, e.g., W and Mo, so they have a greater "natural attraction" towards oxygen (which has an electronegativity of 3.44). So, one expects that these metals have a bigger chance of forming an oxide rather than a carbide. Cr and V are actually in between the two groups (W, Mo, and Fe versus Nb, Ti, Ta, and Hf), which may explain why they tend to first form an oxide, but eventually the carbide phase governs the solid-state transformation. Mn and Zr are exceptions, as we were not able to form a carbide phase for these metals. We must mention that if one would be taking more severe steps to eliminate the presence of oxygen than was done in our work (such as UHV deposition and/or UHV annealing), the necessity of the capping layer might disappear.

When looking at the binary phase diagrams,[17] the first group has carbide phases with a very narrow range of composition (observed as a single vertical line in the phase diagram): W, Mo, Fe, Cr, and Mn. The second group (V, Nb, Ti, Ta, Zr, and Hf) has carbide phases which can be stable within a certain range of carbon concentration. The ranges of composition listed in Table II are estimated from the binary phase diagrams. This broad range of composition of the carbide phase will reflect itself in a change of certain physical properties of the carbide, as C vacancies will act as powerful scattering centers for electrons and phonons. Within the range, there will be a variation of several properties: the lattice parameters and density,[35] Hall coefficient,[36] transition temperature to the superconducting state,[37] coefficient of thermal expansion, magnetic susceptibility, heat of formation, and (technologically important for microelectronics) the

PROOF COPY 100704JAP

PROOF COPY 100704JAP

AQ: #8

TABLE III. The transition metals studied in this work, sorted by electronegativity. The phase sequence for the solid-state reaction are listed in order of appearance. The last two columns indicate for which materials a capping layer is absolutely necessary to obtain carbide formation.

Metal	Electronegativity	Phases	TF-Exp without cap	TF-Exp with cap
W	2.36	W_2C, WC	Carbide	Carbide
Mo	2.16	Mo_2C	Carbide	Carbide
Fe	1.83	Fe_3C	Carbide	Carbide
Cr	1.66	Cr_2C, Cr_3C_{2-x}, Cr_3C_2	Oxide-carbide	Oxide-carbide
V	1.63	VC	Oxide-carbide	Oxide-carbide
Nb	1.60	Nb_2C, NbC	Oxide	Carbide
Mn	1.55		Oxide	Oxide
Ti	1.54	TiC	Oxide	Carbide
Ta	1.5	Ta_2C, TaC	Oxide	Carbide
Zr	1.33	Zr_3O, ZrO	Oxide	Oxide
Hf	1.3	HfC	Oxide	Carbide

PROOF COPY 100704JAP

481 resistivity.[10] It is clear that one has to take this into account, 482 when searching for reliable contacts for semiconductors.

483 Considering the kinetics of the reaction, one can learn 484 from literature that the reaction for carbide formation is dif- 485 fusion controlled, e.g., this was reported for TiC by Peng and 486 Clyne[38] and for Mo_2C by Mikahilov *et al.*[39] Therefore, dif- 487 fusion of one of the species through the growing film will be 488 the rate-controlling mechanism for the reaction. The graphite 489 formation on top of the carbide layer (for Fe–C and Cr–C) 490 supports the concept that the small carbon atoms are diffus- 491 ing fast through the metal (or carbide). Woodford and 492 Chang[40] evidenced that carbon is the only species undergo- 493 ing significant diffusion in the Nb–C system.

494 If one compares the range of composition and the acti- 495 vation energies for the different carbide phases, one would 496 intuitively try to correlate both. One would expect that C 497 atoms will move more easily through a layer with more va- 498 cancies, which may explain the lower activation energy. 499 Many authors[40,41] pose that the activation energy for diffu- 500 sion is independent of the composition. Others[30,32,42] have 501 shown that different carbon diffusion mechanisms are active, 502 and the dominance of a particular mechanism is dependent 503 on the composition and on the temperature range. Due to 504 these different diffusion mechanisms, a variation in the acti- 505 vation energy may occur. Yu and Davis found a different 506 activation energy for single crystals of $NbC_{0.868}$ and 507 $NbC_{0.834}$, compared to the activation energy for $NbC_{0.766}$. 508 This difference was attributed to the presence of a different 509 diffusion mechanism. For NbC_x systems with $x > 0.766$, the 510 carbon atom jumps to a vacant octahedral site in the $\langle 111 \rangle$ 511 direction by a two-step process, called the *O-T-O mecha-* 512 *nism*: first, a shorter $\langle 111 \rangle$ jump to an unoccupied tetrahedral 513 site on the Nb sublattice, followed by an immediate $\langle 111 \rangle$ 514 jump to a vacant octahedral site (i.e., a vacant site on the C 515 sublattice). As the carbon concentration increases, the char- 516 acter of bonding in the material changes, which results in an 517 electronic charge distribution most readily passed by C at- 518 oms jumping in the $\langle 111 \rangle$ direction. For lower carbon con- 519 centrations, the *transient divacancy mechanism* is favored, 520 where the carbon atom jumps to the vacant octahedral site by 521 way of a normally occupied metal vacancy, which has mo- 522 mentarily become associated with the carbon vacancy.

Overviewing our results for the activation energies, we 523 see that the results for TiC, HfC, VC, Nb_2C, Mo_2C, and WC 524 are in the same range of the results of Yu and Davis[32] that 525 were correlated to the *O-T-O mechanism*, while the other 526 results (W_2C, Fe_3C, and NbC) show higher activation ener- 527 gies that correlate better with the *transient divacancy mecha-* 528 *nism*. However, one would have to look at the charge densi- 529 ties of the different compounds, in order to get an idea of the 530 most favored diffusion path, to correlate the activation en- 531 ergy to a certain diffusion mechanism. 532

We stress, however, that other influences such as grain 533 boundary diffusion probably play a role in the diffusion. 534 Barzilai *et al.*[43] wrote that the activation energy values for 535 carbon diffusion in thin layers differ greatly from those ob- 536 tained for bulk materials, and they address their difference in 537 values to the microporosity of the film. It is also well known 538 that the activation energy at grain boundaries (or defects) is 539 different than in bulk material. For carbide formation, the 540 work of Yeh *et al.*[44] and Hatano *et al.*[45] give evidence for this 541 difference. So from this all, one can conclude that grain 542 boundaries and dislocations will play an important role in 543 our growth of carbides. Furthermore, the influence of impu- 544 rities such as oxygen in the (surface) layer, but also nitrogen 545 or other metals, will also have its influence on the diffusion, 546 and hence the activation energy. Matzke[42] writes that defect 547 concentrations are often impurity controlled and that diffu- 548 sion is governed by impurity-defect interactions. 549

As mentioned in the introduction, several criteria should 550 be used to select the best candidate as electric contact to 551 carbon-containing semiconductors. Firstly, the most carbon- 552 rich carbides are thermodynamically stable in contact with 553 an infinite carbon supply. Secondly, one has to take into ac- 554 count the sensitivity towards oxidation, so W, Mo, Fe, Cr, 555 and V come first to mind as promising candidates. They do 556 not have the necessity of a capping layer, which facilitates 557 the fabrication of the contact. Cr and V first form oxides, 558 which may cause problems when more oxygen is available 559 during processing. From the remaining candidates, Mo_2C 560 and Fe_3C have relatively low formation temperatures (W_2C 561 not), which is quite favorable. However, Fe_3C tends to seg- 562 regate a graphite layer, which may interfere with the device 563

PROOF COPY 100704JAP

operation. Mo_2C thus appears as a primary candidate for contacting carbon-containing semiconductors.

Our work focused on the formation of carbides. For practical application as a contacting material to carbon containing semiconductors, the electrical nature of the carbide-semiconductor interface will also be important. Unfortunately, the use of amorphous carbon substrates during most of our experiments did not allow for an investigation of the contact resistance. Undoubtedly, the contact resistance will vary depending on the semiconductor that is used (SiC, diamond, carbon nanotubes,…). For contacts to diamond, Nakanishi *et al.*[46] reported electrical measurements for Mo contacts to boron-doped polycrystalline diamond films. For diamond with a resistivity of 13 Ω cm, they found a contact resistance of $\sim 10^{-2}\ \Omega\ \text{cm}^2$ for as-deposited Mo. Annealing of this sample for 60 min at 600 °C resulted in the formation of Mo_2C and in an improved contact resistance of $\sim 10^{-3}\ \Omega\ \text{cm}^2$. For diamond with a resistivity of 0.08 Ω cm, annealed Mo films resulted in a contact resistance of $\sim 10^{-6}\ \Omega\ \text{cm}^2$. They also report that the Mo_2C contacts were thermally stable and did not deteriorate after annealing at 600 °C for 3 h.

V. CONCLUSION

According to the binary phase diagrams, only 13 transition metals form a stable carbide phase and in this work 11 of these were investigated in their thin film solid-state reaction with carbon. We found that nine of these thin film transition metal-carbon systems (W, Mo, Fe, Cr, V, Nb, Ti, Ta, and Hf) form stable carbide phases through a solid-state reaction with carbon. The necessity of a capping layer for Nb, Ti, Ta, and Hf was discussed. Despite the capping layers, the Mn–C and Zr–C systems did not form carbide phases. The different phases of the solid-state reaction and their transition temperature have been identified using *in situ* XRD, and for some of the phases an activation energy was obtained with kinetic studies, and resistivities of the carbide phases were measured *ex situ*. The results are summarized in Table II. We also mention the unexpected phenomenon of graphite formation on top of the carbide phase, for the Fe–C and the Cr–C systems.

ACKNOWLEDGMENTS

The authors would like to thank R. A. Carruthers for thin film deposition, and J. Jordan-Sweet for help with the XRD beamline. The synchrotron XRD experiments were conducted under DOE Contract No. DE-AC02-76CH-00016. One of the authors (C.D.) acknowledges the Nationaal Fonds voor Wetenschappelijk Onderzoek-Vlaanderen for financial support.

[1] J. A. Cooper and A. Agarwal, Proc. IEEE **90**, 956 (2002).
[2] V. K. Bazhenov, I. M. Vikulin, and A. G. Gontar, Sov. Phys. Semicond. **19**, 829 (1985).
[3] P. Avouris, Chem. Phys. **281**, 429 (2002).
[4] S. L. Zhang and M. Ostling, Crit. Rev. Solid State Mater. Sci. **28**, 1 (2003).
[5] J. J. Gilman, J. Appl. Phys. **41**, 1664 (1970).
[6] E. Furimsky, Appl. Catal., A **240**, 1 (2003).
[7] J. X. Wang, S. F. Ji, J. Yang, Q. L. Zhu, and S. B. Li, Catal. Commun. **6**, 389 (2005).
[8] J. R. Chen, J. Vac. Sci. Technol. A **5**, 1802 (1987).
[9] *International Centre for Diffraction Data (jcpds-icdd)* (1998).
[10] W. S. Williams, JOM **49**, 38 (1997).
[11] A. K. Schaper, H. Q. Hou, A. Greiner, and F. Phillipp, J. Catal. **222**, 250 (2004).
[12] N. Lundberg, M. Ostling, C. M. Zetterling, P. Tagtstrom, and U. Jansson, J. Electron. Mater. **29**, 372 (2000).
[13] M. Y. Liao and Y. Koide, J. Vac. Sci. Technol. B **24**, 185 (2006).
[14] A. K. Chaddha, J. D. Parsons, and G. B. Kruaval, Appl. Phys. Lett. **66**, 760 (1995).
[15] T. Tachibana, B. E. Williams, and J. T. Glass, Phys. Rev. B **45**, 11975 (1992).
[16] R. Martel, V. Derycke, C. Lavoie, J. Appenzeller, K. K. Chan, J. Tersoff, and P. Avouris, Phys. Rev. Lett. **87**, ■ (2001).
[17] T. B. Massalski, Metall. Trans. B **20**, 445 (1989).
[18] K. L. Moazed, J. R. Zeidler, and M. J. Taylor, J. Appl. Phys. **68**, 2246 (1990).
[19] A. Bachli, J. Chen, R. Ruiz, and M.-A. Nicolet, in MRS Symposium Proceedings, ■, ■ (unpublished), Vol. 339, p. 247.
[20] W. P. Leroy, C. Detavernier, R. L. Van Meirhaeghe, A. J. Kellock, and C. Lavoie, J. Appl. Phys. **99**, ■ (2006).
[21] E. G. Colgan and F. M. d'Heurle, J. Appl. Phys. **79**, 4087 (1996).
[22] C. P. Buhsmer and P. H. Crayton, J. Mater. Sci. **6**, 981 (1971).
[23] H. Romanus, V. Cimalla, J. A. Schaefer, L. Spiess, G. Ecke, and J. Pezoldt, Thin Solid Films **359**, 146 (2000).
[24] A. Santaniello, W. Moller, and J. Roth, J. Appl. Phys. **65**, 3400 (1989).
[25] A. Santaniello, J. Appelt, J. Bohdansky, and J. Roth, Nucl. Instrum. Methods Phys. Res. B **19–2**, 80 (1987).
[26] R. Sinclair, T. Itoh, and R. Chin, Microsc. Microanal. **8**, 288 (2002).
[27] D. E. Jiang and E. A. Carter, Phys. Rev. B **71**, ■ (2005).
[28] E. Bouzy, G. Lecaer, and E. Bauergrosse, Philos. Mag. Lett. **64**, 1 (1991).
[29] L. Ramqvist, K. Hamrin, G. Johansson, A. Fahlman, and C. Nordling, J. Phys. Chem. Solids **30**, 1835 (1969).
[30] C. R. Guarnieri, F. M. Dheurle, J. J. Cuomo, and S. J. Whitehair, Appl. Surf. Sci. **53**, 115 (1991).
[31] S. Barzilai, N. Frage, and A. Raveh, Surf. Coat. Technol. **200**, 4646 (2006).
[32] B. B. Yu and R. F. Davis, J. Phys. Chem. Solids **40**, 997 (1979).
[33] W. Lengauer, J. Alloys Compd. **229**, 80 (1995).
[34] J. S. Chen, E. Kolawa, M. A. Nicolet, and F. S. Pool, Thin Solid Films **236**, 72 (1993).
[35] A. L. Bowman, J. Phys. Chem. **65**, 1596 (1961).
[36] W. S. Williams, Phys. Rev. **135**, A505 (1964).
[37] A. L. Giorgi, E. G. Szklarz, E. K. Storms, A. L. Bowman, and B. T. Matthias, Phys. Rev. **125**, 837 (1962).
[38] X. L. Peng and T. W. Clyne, Thin Solid Films **293**, 261 (1997).
[39] S. N. Mikhailov, D. Ariosa, J. Weber, Y. Baer, W. Hanni, X. M. Tang, and P. Alers, Diamond Relat. Mater. **4**, 1137 (1995).
[40] J. Woodford and Y. A. Chang, Metall. Mater. Trans. A **29**, 2717 (1998).
[41] F. J. J. Vanloo, W. Wakelkamp, G. F. Bastin, and R. Metselaar, Solid State Ionics **32–3**, 824 (1989).
[42] H. Matzke, Solid State Ionics **12**, 25 (1984).
[43] S. Barzilai, A. Raveh, and N. Frage, Vacuum **79**, 171 (2005).
[44] J. J. Yeh, R. L. Pfeffer, M. W. Cole, M. Ohring, and J. E. Yehoda, Diamond Relat. Mater. **5**, 1195 (1996).
[45] Y. Hatano, M. Takamori, K. Nogita, K. Matsuda, S. Ikeno, and K. Watanabe, J. Nucl. Mater. **337–339**, 902 (2005).
[46] J. Nakanishi, A. Otsuki, T. Oku, and O. Ishiwata, J. Appl. Phys. **76**, 2293 (1994).
[47] L. Toth, in *Transition Metal Carbides and Nitrides*, Refractory Materials, A Series of Monographs Vol. 7 (Academic, New York, 1971).
[48] H. J. Goldschmidt, *Interstitial Alloys* (Butterworths, London, 1967).
[49] M. Karapet'yants and M. Karapet'yants, *Thermodynamic Constants of Inorganic and Organic Compounds* (Ann Arbor-Humphrey, London, 1970).

PROOF COPY 100704JAP

AUTHOR QUERIES — 100704JAP

#1 Au: Pls. supply the postal code for the 2nd location
#2 Au: Pls. define “SALICIDE”
#3 Au: Pls. supply page no. in Refs. 16 & 20
#4 Au: Pls. supply city & dates of conference in Ref. 19
#5 Au: Pls. update Ref. 19
#6 Au: Pls. supply page no. in Ref. 27
#7 Au: Pls. check changes from “hex.” to “hexagonal,” “orth.” to “orthorambic,” & “compl. cub.” to “complex cubic”
#8 Au: Pls. define “TF-Exp”

PROOF COPY 100704JAP